Extended linear polarimeter to measure retardance and flicker: application to liquid crystal on silicon devices in two working geometries

Francisco J. Martínez,[a,b] Andrés Márquez,[a,b,*] Sergi Gallego,[a,b] Jorge Francés,[a,b] and Inmaculada Pascual[b,c]
[a]Universidad de Alicante, Dept. de Física, Ing. de Sistemas y T. Señal, Ap. 99, Alicante, E-03080, Spain
[b]Universidad de Alicante, I.U. Física Aplicada a las Ciencias y las Tecnologías, Ap. 99, Alicante, E-03080, Spain
[c]Universidad de Alicante, Dept. de Óptica, Farmacología y Anatomía, Ap. 99, Alicante, E-03080, Spain

Abstract. We focus on the evaluation of the applicability of the classical and well-established linear polarimeter to the measurement of linear retardance in the presence of phase flicker. This analysis shows that there are large errors in the results provided by the linear polarimeter when measuring the linear retardance of a device. These errors depend on the specific retardance value under measurement. We show that there are some points where this limitation can be used to measure the fluctuation amplitude consistently. An elegant method is further proposed, enabling the measurement of the average retardance value, thus extending the applicability of the classical linear polarimeter. Experimental characterization results are provided for various electrical sequences addressed onto a parallel aligned liquid crystal on silicon (LCoS) display. Good agreement is obtained with experiment, thus validating the linear polarimeter methodology proposed. Furthermore, results are provided for the LCoS in two reflection geometries, perpendicular incidence with and without nonpolarizing beam splitter, demonstrating robustness of the method. As a result, the evaluation of both phase modulation range and flicker magnitude for any electrical sequence addressed can be easily obtained, which is very important for optimal use of LCoS displays in applications. [DOI: 10.1117/1.OE.53.1.014105]

Keywords: polarimeter; retardance measurement; liquid crystal on silicon displays; parallel aligned; phase-only modulation; spatial light modulation; flicker; diffractive optics.

Paper 131700P received Nov. 5, 2013; revised manuscript received Dec. 20, 2013; accepted for publication Dec. 24, 2013; published online Jan. 21, 2014.

1 Introduction

Liquid crystal (LC) microdisplays have become a central device in a wide range of applications requiring spatial modulation of a wavefront, like in diffractive optics,[1] optical storage,[2] or optical metrology.[3] Liquid crystal on silicon (LCoS) displays have become the most attractive microdisplays for these applications due to their very high spatial resolution and very high light efficiency.[4,5] However, several authors[6–11] have detected that LCoS displays produce a certain amount of phase flicker and/or depolarization. Among the different LCoS technologies typically available, parallel aligned LCoS (PA-LCoS) are especially interesting since they allow easy operation as phase-only devices without coupled amplitude modulation. They can be thought of as variable linear retarders; therefore, for incident linearly polarized light along their neutral lines, no depolarization operation is available; however, they may still exhibit phase fluctuations. This is, for example, the case for digitally addressed devices[12] due to the pulsed nature of the voltage signal addressed.[13,14] In these devices, if the digital sequence format is properly chosen, fluctuations can be significantly decreased to acceptable levels.[15] To this goal, a proper characterization not only of the phase modulation, but also of the amount of phase flicker in the optical signal needs to be done. This reasoning is not restricted to PA-LCoS devices, but it can be applicable, in general, to electrooptic variable linear retarders, such as the novel device proposed by Ramirez et al.[16]

Different measurement methods have been proposed and demonstrated to characterize the phase-shift versus voltage in LCDs and LCoS devices.[12,17,18] Among these methods, the diffractive-based technique used by Lizana et al. in Refs. 12 and 17 allow for instantaneous phase-shift values measurement. In the case of parallel aligned devices, they are totally characterized by their linear retardance versus voltage values. Additional methods typically used in the characterization of wave plates become available to measure the linear retardance. The most popular are ellipsometric, polarimetric, and interferometric ones. In interferometric methods, we need a device introducing a carrier reference signal (heterodyne interferometry), such as an He-Ne Zeeman laser[19] or an electrooptic light modulator[20] working in the common-path geometry.[21] We can also have some element producing a phase-shift between the ordinary and extraordinary components of a beam (phase-shifting interferometry), such as a birefringent wedge.[22] Polarimetric methods of a high precision generally rely on null measurements, such as in the Senarmont compensator.[23,24] Other methods are based on the variation of the intensity when we change the angle of the elements in the polarimeter.[25–29] One common property of all these methods is that they assume that the birefringence in the wave plate has a constant value, no fluctuations, during the measurement process.

*Address all correspondence to: Andrés Márquez, E-mail: andres.marquez@ua.es

0091-3286/2014/$25.00 © 2014 SPIE

Recently some techniques to evaluate the average retardance in the presence of fluctuations in linear retarders have been demonstrated by our group[15] and by Ramirez et al.,[30] based, respectively, on the classical linear polarimeter and on a combination of linear and circular polarimeters. The linear polarimeter technique in Ref. 15 can be implemented by any lab since it basically needs two linear polarizers and a radiometer and only two sets of measurements are necessary to extract the retardance and flicker values. In Ref. 15, we concentrated on the proposal of the characterization technique, but we did not provide the deeper insight, which is actually needed to evaluate the range of validity of the linear polarimeter in the presence of phase flicker. Furthermore, the technique was presented for the combined system composed of the LCoS and a beam splitter in front.

In the present work, we perform a complete analysis of the applicability of the linear polarimeter to the measurement of linear retardance in the presence of phase flicker. This deeper insight allows us to clearly define a valid and accurate methodology enabling the use of the classical linear polarimeter to a new range of samples. First, in Sec. 2 we show the basic theory for the linear polarimeter, its limitations, and its extension to samples exhibiting phase flicker. In Sec. 3, we proceed with the instantaneous and average measurements, using a PA-LCoS display and for various electrical sequences. We also consider two working geometries, with beam splitter and in quasiperpendicular incidence, in order to verify the validity of the measurements and technique in two typical configurations. Eventually, the main conclusions are given in Sec. 4.

2 Theory: Linear Polarimeter and Phase Flicker

2.1 *Limitations in the Presence of Instabilities*

The total retardance Γ of a wave plate is given by

$$\Gamma = \frac{2\pi\Delta n(\lambda)d}{\lambda}, \tag{1}$$

where λ is the wavelength of the incident light, $\Delta n(\lambda)$ is the difference between the extraordinary and the ordinary index of the birefringent material (e.g., the LC) at this wavelength, and d is the thickness of the wave plate. In general, most of the measurement methods provide the retardance value Γ_0 modulo 2π, which is given by $\Gamma = \Gamma_0 + m2\pi$, where m is an integer, called the order of the wave plate. In the case of the zero-order wave plate, $m = 0$ and $\Gamma_0 = \Gamma$, which is the case in many LCoS since thinner devices produce a faster response.

The measurement method we propose is based on the linear polarimeter,[25–29] where the device under test, the linear retarder or wave plate, is situated between two linear polarizers (see Fig. 1), illuminated with a monochromatic laser source. In the basic configuration, there is a radiometer at the output of the polarimeter.

By means of the procedure developed in Refs. 15 and 29, we know that a robust measurement of the retardance value Γ is obtained from intensity measurements for polarizers with their transmission axis oriented at ± 45 deg with respect to the neutral lines of the wave plate. The polarizers can still be parallel or perpendicular to each other, thus producing, respectively, the following intensity measurements:

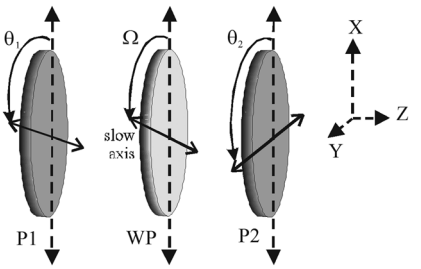

Fig. 1 Linear polarimeter with the wave plate WP to be measured. P1 and P2 are the polarizers.

$$I_{\mathrm{OUT}}^{\parallel} = \frac{I_0}{2}[1 + \cos\,\Gamma], \tag{2}$$

$$I_{\mathrm{OUT}}^{\perp} = \frac{I_0}{2}[1 - \cos\,\Gamma]. \tag{3}$$

The retardance value is contained in the cosine function, which can be properly isolated.

$$\cos\,\Gamma = \frac{I_{\mathrm{OUT}}^{\parallel} - I_{\mathrm{OUT}}^{\perp}}{I_{\mathrm{OUT}}^{\parallel} + I_{\mathrm{OUT}}^{\perp}}. \tag{4}$$

Finally, the retardance value Γ is given as

$$\Gamma = \cos^{-1}\left(\frac{I_{\mathrm{OUT}}^{\parallel} - I_{\mathrm{OUT}}^{\perp}}{I_{\mathrm{OUT}}^{\parallel} + I_{\mathrm{OUT}}^{\perp}}\right). \tag{5}$$

Measurements given in Eqs. (2) and (3) are probably the most typically used ones to obtain the retardance in linear retarder devices. Next, we want to analyze the range of applicability of the classical linear polarimeter in the presence of instabilities or fluctuations in the linear retardance. To incorporate them, let us consider a triangular profile for the variation of retardance with time $\Gamma(t)$ (see Fig. 2). This is a reasonable assumption in the case of PA-LCoS as can be seen from the instantaneous measurement plots that we show in Sec. 3.1., which as a first approximation exhibit a triangular shape. Furthermore, the triangular time-dependent profile represents actually a linear model; thus, the first option to try before more complex approaches may be proven necessary. The triangular profile can be analytically expressed by the following equation:

$$\Gamma(t) = \begin{cases} \bar{\Gamma} - a + \frac{2a}{T/2}t & 0 \le t < T/2 \\ \bar{\Gamma} + 3a - \frac{2a}{T/2}t & T/2 \le t < T \end{cases}, \tag{6}$$

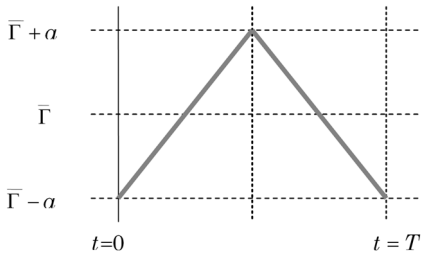

Fig. 2 Triangular profile considered for the temporal fluctuation of the linear retardance.

where $\bar{\Gamma}$ and a are, respectively, the values for the average retardance and its fluctuation amplitude, and T is the period for the fluctuation instability.

To calculate the average value in Eqs. (2) and (3), we average the cosine and obtain

$$\langle \cos \Gamma(t) \rangle = \frac{\sin(a)}{a} \cos(\bar{\Gamma}), \tag{7}$$

where we appreciate the appearance of the $\sin c$ term modulating the cosine function. Equations (2) and (3) may be rewritten in terms of the average value and the fluctuation amplitude as follows:

$$\langle I^{\parallel}_{\mathrm{OUT}} \rangle = \frac{I_0}{2}\left[1 + \frac{\sin a}{a}\cos \bar{\Gamma}\right], \tag{8}$$

$$\langle I^{\perp}_{\mathrm{OUT}} \rangle = \frac{I_0}{2}\left[1 - \frac{\sin a}{a}\cos \bar{\Gamma}\right]. \tag{9}$$

Let us now combine Eqs. (8) and (9) to remove the normalization factor to obtain the following expression:

$$\frac{\langle I^{\parallel}_{\mathrm{OUT}} \rangle - \langle I^{\perp}_{\mathrm{OUT}} \rangle}{\langle I^{\parallel}_{\mathrm{OUT}} \rangle + \langle I^{\perp}_{\mathrm{OUT}} \rangle} = \frac{\sin a}{a} \cos \bar{\Gamma}. \tag{10}$$

Eventually, the average retardance $\bar{\Gamma}$ is obtained by inverting Eq. (10).

$$\bar{\Gamma} = \cos^{-1}\left[\frac{(\langle I^{\parallel}_{\mathrm{OUT}} \rangle - \langle I^{\perp}_{\mathrm{OUT}} \rangle)/(\langle I^{\parallel}_{\mathrm{OUT}} \rangle + \langle I^{\perp}_{\mathrm{OUT}} \rangle)}{\sin a/a}\right]. \tag{11}$$

In the case when no fluctuations exist ($a = 0^o$), Eqs. (8) to (11) transform into the classical results already given in Eqs. (2) to (5).

To analyze the range of validity for the classical linear polarimeter in the presence of phase flicker, we perform the following simulated experiment. We apply Eqs. (8) and (9) to calculate the experimental intensity values measured in the presence of fluctuations in the retardance. The retardance value is recovered using Eq. (5), which is the classical expression that does not take into account the existence of fluctuations. Analytically, the simulated experiment consists of applying Eq. (5) onto the experimental result given by Eq. (10), that is,

$$\bar{\Gamma}_{\mathrm{calc}} = \cos^{-1}\left[\frac{\sin a}{a} \cos(\bar{\Gamma}_{\mathrm{true}})\right], \tag{12}$$

where $\bar{\Gamma}_{\mathrm{calc}}$ is the calculated retardance, and $\bar{\Gamma}_{\mathrm{true}}$ and a are the input values considered for the retardance and fluctuation, respectively. In Fig. 3, we show the calculated retardance $\bar{\Gamma}_{\mathrm{calc}}$ as a function of the true retardance $\bar{\Gamma}_{\mathrm{true}}$, and for various fluctuation amplitudes a, indicated on the plot. In Fig. 3, we represent the wrapped phase values in the range 0 to 180 deg, which is the definition dominium for the $\cos^{-1}$ function in Eq. (12).

First thing we note is that maxima and minima, the extremals, in the calculated retardance occur at values multiple of 180 deg of the true retardance independent of the flicker magnitude. We observe that there exist clear

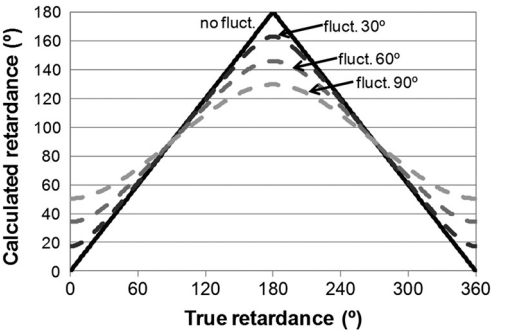

Fig. 3 Simulation of the retardance measurement experiment in the presence of fluctuations considering the classical linear polarimeter. The calculated retardance is obtained applying the classical expression, i.e., not taking into account the fluctuations introduced in the simulation, indicated in the plots (30, 60, and 90 deg). The calculated retardance coincides with the true retardance in the case of no fluctuations (continuous line).

deviations between the calculated and the true retardance, and the amount of this deviation varies largely as a function of the true retardance value. The deviations magnify at true retardance values multiple of 180 deg. Outside of these points and if the fluctuation amplitude is not very large, we find that the calculated values are very close to the true retardance values. This allows us to say that the classical method may still be valid in many cases. We note that, in general, the fluctuation amplitude is not known, thus making impractical the application of Eq. (11), which, according to the linear model developed, should provide the correct values for the retardance. Then it is necessary to develop a method to calculate the amplitude of the phase flicker. This is done in the next section.

2.2 *Extended Linear Polarimeter for Phase Flicker Characterization*

We have seen in Fig. 3 that maxima and minima, extremal points, in the calculated retardance occur at values multiple of 180 deg of the true retardance independent of the flicker magnitude. This invariance allows the *a priori* knowledge for the average retardance at these points, enabling to calculate the magnitude of the fluctuation amplitude a at these maxima and minima. This can be easily deduced from a close examination of Eq. (10). From this expression we see that, in general, the intensity measurements are both dependent on the average retardance $\bar{\Gamma}$ and the fluctuation amplitude a; thus they cannot be uncoupled with only the parallel and crossed polarizers intensity measurements. Yet at the extremals, the retardance value is known; it is a multiple of 180 deg, and the intensity measurements become only dependent on the fluctuation amplitude a; then its value can be obtained. Afterward the amplitude a can be introduced in Eq. (11) to produce a more accurate estimation of the average retardance $\bar{\Gamma}$.

To obtain the fluctuation amplitude a, the deviation between calculated and true retardance values can be used. If we apply Eq. (11) at the extremals, where the true retardance value is multiple of 180 deg, we find that the absolute retardance difference Γ_{diff} between the calculated and the true retardance value is given by

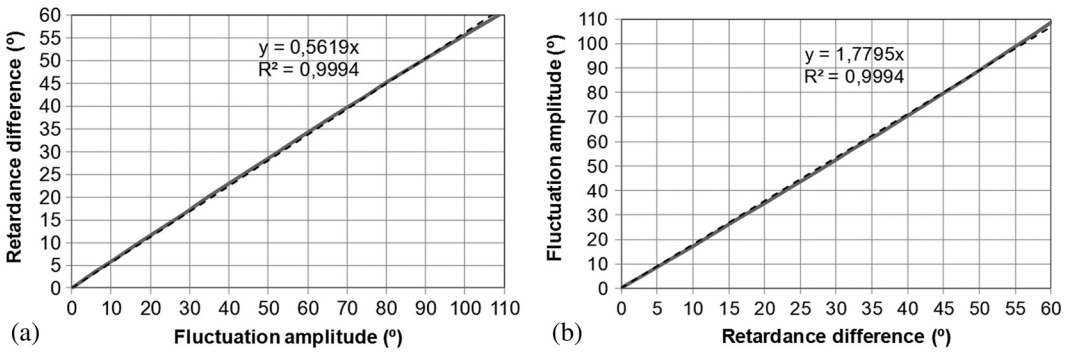

Fig. 4 (a) Retardance difference with respect to the ideal $a = 0$ deg as a function of the fluctuation amplitude, at retardance points multiple of 180 deg. (b) Reverse relation, valid to estimate the magnitude of the fluctuation amplitude. We observe the goodness of the linear fit for the range of values considered in the plot.

$$\Gamma_{\text{diff}} = \cos^{-1}\left(\frac{\sin a}{a}\right). \tag{13}$$

Let us represent in Fig. 4(a) the absolute retardance difference Γ_{diff} [Eq. (13)] as a function of the fluctuation amplitude a. We see that for a fluctuation amplitude range till $\tilde{1}10$ deg, which is a reasonably high value, the retardance difference Γ_{diff} increases with a high linearity (dashed line; fitting equation written on the plot). If the coordinates for the values in Fig. 4(a) are reversed, then we obtain Fig. 4(b). This plot enables to estimate the magnitude of the fluctuation a from the value of the retardance difference Γ_{diff} exhibited at the extremals. For the retardance difference range considered, the relation is highly linear. On the figure we show (dashed line) the linear fit to the curve. For the sake of completeness, we show the squared correlation factor, which is very close to one. Using this linear relation, we can quantitatively obtain the magnitude of the fluctuation from the value of Γ_{diff}.

We note that other alternatives to estimate the magnitude of the fluctuation amplitude are possible, such as in Ref. 15. However, some advantages are given by the procedure given in this paper, which is based on the discussion of the simulated experiment presented in Fig. 3. On one side, we play directly with the retardance values, what offers a direct insight to estimate how accurate the retardance returned by the classical linear polarimeter procedure may be. This can be qualitatively inferred from the deviation between calculated and true retardance in Fig. 3. On the other side, the quantitative applicability of the technique, when calculating the fluctuation amplitude, is greatly enhanced since we can work with linear relations, as we have seen in Fig. 4(b). Once the amplitude of the fluctuation a has been obtained, then Eq. (11) can be used to obtain the average retardance $\bar{\Gamma}$.

3 Results and Discussion

3.1 *Experiment*

We consider the characterization of a PA-LCoS in two of the typical working geometries:[31] perpendicular incidence with a beam splitter in front and quasiperpendicular incidence (no beam splitter is necessary in front of the LCoS). In Fig. 5, the experimental setup for the case with the beam splitter in front of the LCoS is presented. It basically consists of a light source (He-Ne laser producing linearly polarized light at $\lambda = 633$ nm), the device under test (reflective LCoS), and the necessary input and output linear polarizers, which are used in parallel or crossed configuration, and some intensity measuring device (radiometer). A quarter wavelength wave plate is added after the laser to assure that enough intensity passes through the first polarizer. We introduce two nonpolarizing cube beam splitters (NPBS, model 10BC16NP.4, from Newport): one of them to separate the incident and reflected beams from the LCoS and the other to enable amplitude division with a 50/50 ratio of the reflected beam so that crossed and parallel intensity can be measured simultaneously (thus, two radiometers are introduced). This further enables synchronized measurement of the instantaneous parallel and crossed polarizer intensity values simply by connecting the two radiometers to the two channels of an oscilloscope (shown in the figure). The same setup is therefore valid for the characterization of the average and the instantaneous values. For the other working geometry considered in this work, quasiperpendicular incidence, the only change introduced is the removal of the beam splitter in front of the LCoS, and the beam impinges quasiperpendicularly onto the LCoS so that the incident and reflected beams become spatially separated.

In the experiments performed, the input polarizer transmission axis is at $+45$ deg to the vertical of the lab, which is the x axis of our reference system as shown in Fig. 1. The director for the liquid crystal (i.e., the extraordinary axis) in the LCoS is oriented along the horizontal, i.e., at $+90$ deg with respect to the x axis. The director axis in nematic filled devices, as it is the case for our LCoS, typically corresponds to the slow axis. In the first working geometry, light impinges perpendicularly onto the LCoS and onto the two beam splitters. Perpendicular incidence onto the beam splitters is important so that they do not introduce polarization effects on their own. In the second working geometry, the beam splitter in front of the LCoS is removed and the beam incides at quasiperpendicular incidence (~ 3 deg). Typically the angular uncertainty on the orientation of the input and output polarizers with respect to the neutral lines of the LCoS can be considered ± 1 deg.

We note that the method proposed in Sec. 2 can be applied to any electrooptic variable linear retarder. In this paper, we focus our attention on phase-only LCoS devices. We consider a modern electrically controlled birefringence LCoS display. Some of its technical specifications are as follows:

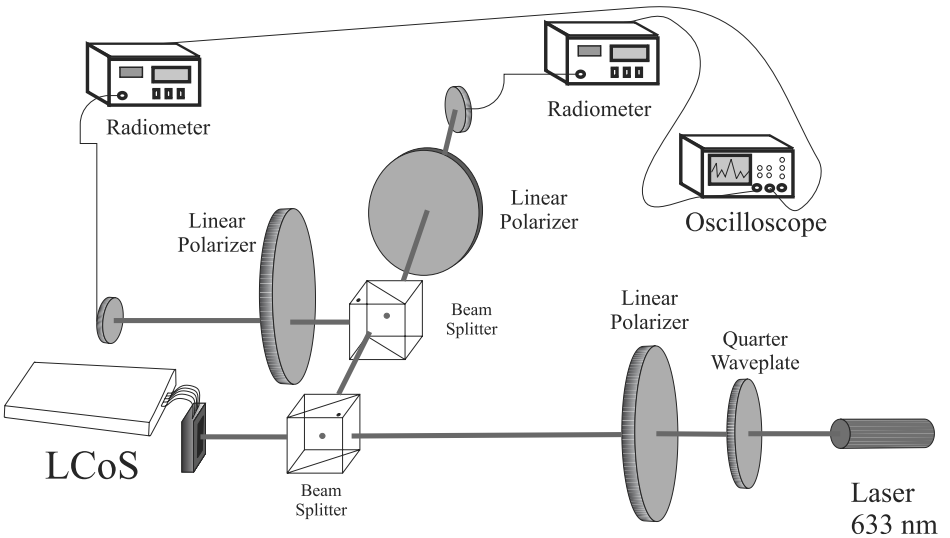

Fig. 5 Experimental setup for the working geometry corresponding to perpendicular incidence onto the liquid crystal on silicon with a beam splitter in front. The setup allows to measure both average and instantaneous values.

1920×1080 pixels, 0.7" diagonal, 8.0 μm of pixel pitch, and with a fill factor of 87%. It is a digitally addressed LCoS device. Different digital addressing sequences[13,14] can be generated by the driver electronics. In particular, we will evaluate three addressing sequences, whose configuration files are provided with the software for the display, whose labels indicate their main properties: 18-6 default, 18-6 2pi linear 633 nm, and 5-5 2pi linear 633 nm. The first number indicates the quantity of equally weighted bit-planes, and the second number the quantity of binary bit-planes.[13] This means that the sequence 18-6 is longer than the one corresponding for the sequence 5-5. In principle, for shorter sequences, the flicker gets smaller.[13] However, a larger sequence provides a larger number of possible phase levels: $(18+1) \times 2^6 = 1216$ for the sequence 18-6 and $(5+1) \times 2^5 = 192$ for the sequence 5-5. In principle, the sequences 18-6 2pi linear 633 nm and 5-5 2pi linear 633 nm have been, respectively, optimized for the wavelength 633 nm to provide a phase depth of 2π radians, and quite a linear relation between phase value and gray level. Sequence 18-6 default is a nonoptimized configuration, where the applied voltage range is not restricted to provide a 2π radians phase depth and reduction of fluctuations have not been taken care of. Therefore, it is a good configuration to test the theory and methodology presented in the paper. Using these three different sequences, we can evaluate different levels of flicker and ranges of retardance.

3.2 *Instantaneous Retardance Measurements*

As previously stated, the experimental setup enables the synchronized measurement of the parallel and crossed polarizer intensities in real time, connected to a two-channel oscilloscope. Thus, we can obtain the instantaneous retardance value as a function of time for a fix gray-level value. This real-time capability is interesting in order to evaluate the profile for the instabilities. Furthermore, the instantaneous values can be used to calculate the average retardance and its amplitude fluctuation, and these values can be compared with the ones obtained applying the extended linear polarimeter approach presented in Sec. 2.

In particular, we have proceeded with the measurement of the instantaneous retardance for a series of gray levels (0, 100, 200, and 255), which sample the applicable voltage range. Results are shown in Figs. 6(a) to 6(c), respectively, for the sequences 18-6 default, 18-6 2pi linear 633 nm, and 5-5 2pi linear 633 nm for the first working geometry (with NPBS), and in Figs. 6(d) to 6(f) for the second working geometry (quasiperpendicular). We obtain that the time period (frequency) for the fluctuations in our PA-LCoS device is 8.66 ms (120 Hz). In the different plots we see that there are no visible oscillations for gray level 0. For the other gray levels, the periodic temporal evolution actually resembles in a first approximation a triangular profile, as considered in the model according to Fig. 2, even though, in general, the profile is composed of various subpeaks within each period, probably due to the pulsed nature of the digital sequence applied. This substructure varies for the various gray levels within a graph. It is also visible that the amplitude of the oscillations is smaller for the sequence 5-5 2pi linear 633 nm and clearly larger for 18-6 default. Actually, in the latter sequence, the oscillations clearly expand out of 0 to 180 deg dominium of definition for the $\cos^{-1}$ function: they are represented as folded against the 0-deg ordinate and 180-deg ordinate since we do not have a consistent criterion to unfold the values. Comparison between the results for the two working geometries show that basically the values obtained are not influenced by the insertion of the NPBS (first working geometry) or by the nonperpendicular incidence (second working geometry).

From the measurements in Fig. 6, we have elaborated Table 1, where we show quantitative values for the average retardance and its corresponding fluctuation amplitude, calculated as the half peak-to-peak amplitude of the temporal oscillation. No results are shown for the sequence 18-6 default since we do not have a consistent criterion to unfold the retardance values to obtain the average retardance and its amplitude. The same happens for some of the gray levels for

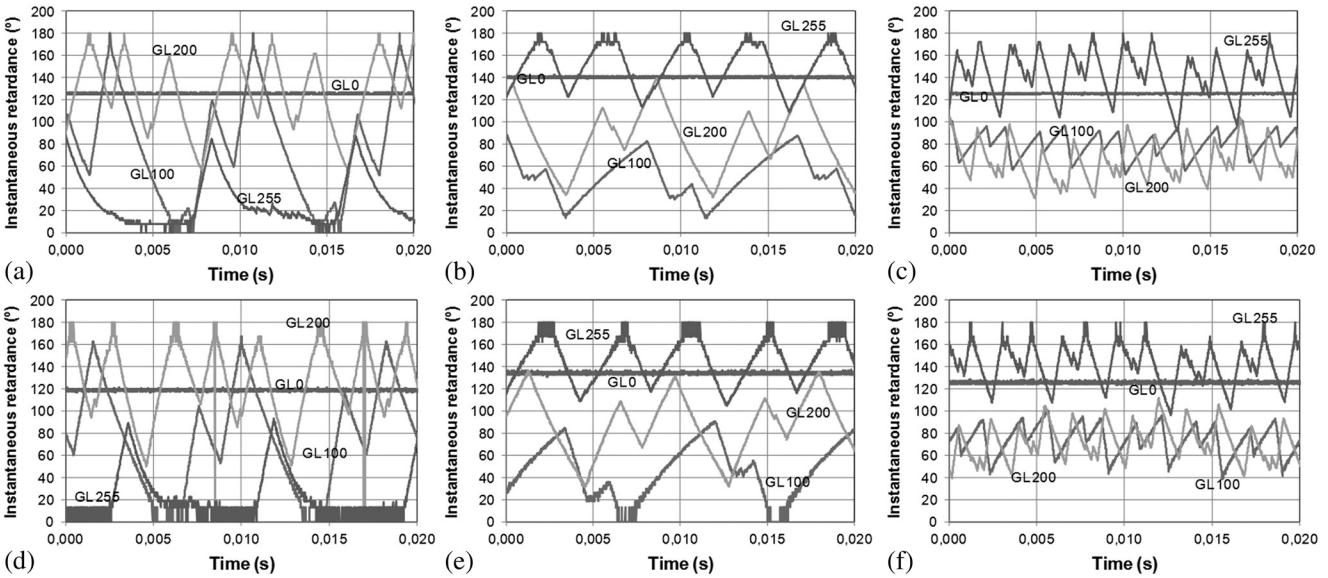

Fig. 6 Temporal evolution of the retardance at gray levels 0, 100, 200, and 255, indicated on the figure. (a) and (d) 18-6 2pi linear 633 nm; (b) and (e) 18-6 2pi linear 633 nm; (c) and (f) 5-5 2pi linear 633 nm. First and second rows correspond, respectively, to the nonpolarizing cube beam splitter (NPBS) and to the quasiperpendicular working geometries.

Table 1 Values for the average retardance and the magnitude of the amplitude of its fluctuation extracted from the instantaneous retardance measurements shown in Fig. 6.

Sequence	Gray level	With NPBS Avg.Ret. ± Fluct. (deg)	Quasiperpendicular Avg.Ret. ± Fluct (deg)
18_6 linear	0	141 ± 2	135 ± 3
	100	51 ± 37	—
	200	86 ± 54	79 ± 57
	255	—	—
5_5 linear	0	125 ± 1	126 ± 2
	100	77 ± 24	75 ± 31
	200	67 ± 37	85 ± 53
	255	—	—

the two sequences presented in Table 1. We see that fluctuation amplitude increases with the gray level. Values of retardance and fluctuation are, in general, quite similar between the two working geometries. Fluctuation is slightly larger for the sequence 18-6 2pi linear 633 nm in comparison with the sequence 5-5 2pi linear 633 nm.

3.3 *Average Retardance and Flicker Evaluation*

Typically, intensity measurements provided by radiometers correspond to the integrated value in a time interval much larger than the few milliseconds period observed in the fluctuating signals in Fig. 6. In Figs. 7(a) and 7(c), we show this averaged intensity values measured for parallel (continuous) and crossed (dashed) polarizers as a function of gray level applied to the LCoS and for the three electrical sequences. Using these curves and applying Eq. (5), we obtain the calculated average retardance represented in Figs. 7(b) and 7(d). First and second rows correspond, respectively, to the NPBS and to the quasiperpendicular working geometries. The analysis of the intensity curves (first column) was the focus of the work we presented in Ref. 15. In the present paper, we get a more complete and straightforward analysis by focusing on the retardance results (second column). We see that the calculated retardance oscillates with maxima and minima clearly separated from values 0 or 180 deg, which according to simulation in Fig. 3 indicate the existence of phase fluctuations. Retardance difference Γ_{diff} at maxima and minima is larger for the sequence 18-6 default when compared with the other two sequences, indicating that fluctuations are also larger. We also see that there is an additional extremal for the sequence 18-6 default, which means that the retardance range is 180 deg larger than for the other two sequences. We note the quantization steps in the case of the sequence 5-5 2pi linear 633 nm, more visible in Fig. 7(a), due to the limited number of levels, which is <256. In the case of the sequence 18-6 default, we observe a series of peaks in the gray-level interval of 150 to 200, which is probably reflecting the switching off and on of different bits in the pulsed signal as the gray level is increased.

From the retardance difference Γ_{diff} at the extremals and taking into account the linear equation in Fig. 4(b), we can obtain an estimation of the fluctuation amplitude. In Table 2, we show under the column "average values" both the retardance difference Γ_{diff} and the estimated fluctuation amplitude at the various extremals, whose gray-level position is indicated in parentheses. The values are given for the three sequences and for the two working geometries. Let us comment the results for the NPBS geometry. We see that at the first extremal, fluctuations are small. In the second extremal, the sequence 18-6 2pi linear 633 nm contains a

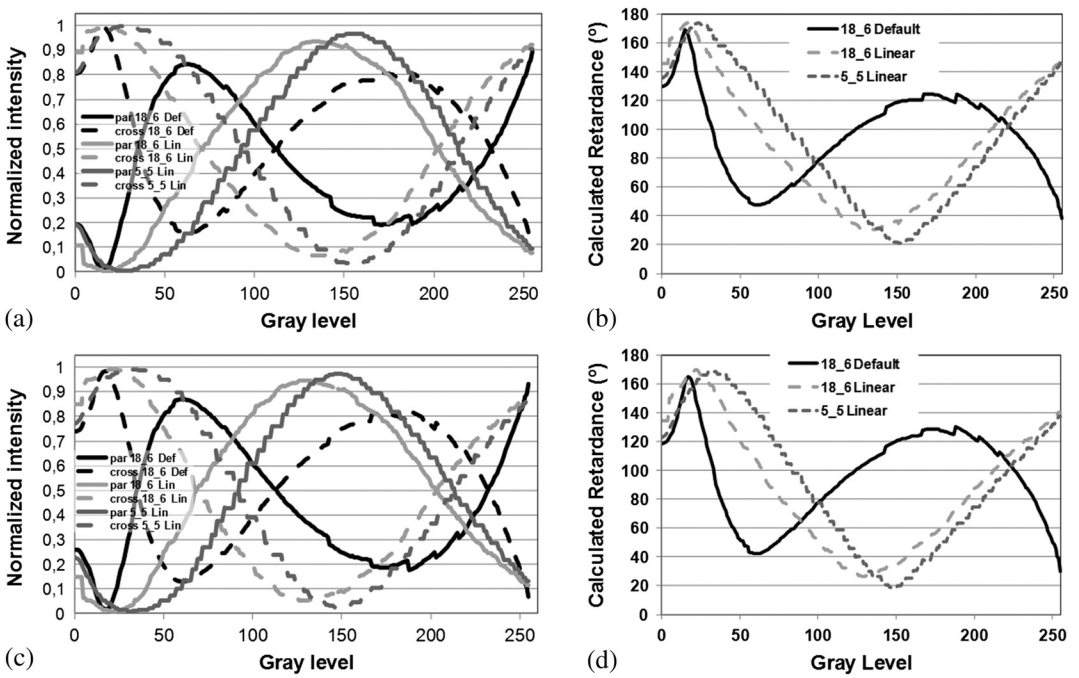

Fig. 7 Intensity measurements for parallel and crossed polarizers [(a) and (c)], and retardance calculations [(b) and (d)], given by the classical expression in Eq. (5). (a) and (b) correspond to the setup with the NPBS. (c) and (d) correspond to the quasiperpendicular incidence.

fluctuation amplitude of ~52 deg, whereas the sequence 5-5 2pi linear 633 nm stays at ~38 deg. Fluctuation amplitude in the case of the sequence 18-6 default at its second and third extremals are 84 and 92 deg, which are very large values indeed. Results are quite comparable with the ones presented for the quasiperpendicular geometry.

To validate the fluctuation amplitudes predicted from the average values, shown in Table 2, next we measure the instantaneous retardance values, as done in Sec. 3.1, applying the gray levels where the extremals are located. In Figs. 8(a) and 8(b), respectively, for the first and second working geometries, we show the temporal evolution of the retardance for each of the sequences at the gray levels where the second extremal is produced, indicated on the figure. The oscillation amplitude is larger for the sequence 18-6 default. We note that the results shown in Fig. 8 are the folded values against the 0-deg ordinate. In these figures, we have a criterion to unfold the instantaneous retardance since we know that the average value is in any case close to 0 deg; thus half of the peaks should be folded against the 0-ordinate axis. Taking this into account, the fluctuation amplitude actually corresponds to the peak value in each of the curves. These values are written in the column "inst. values" in Table 2. When comparing the results in column "average values" and "inst. values," we see that there is a good agreement between the fluctuation amplitude obtained with the

Table 2 Comparison between the fluctuation amplitude *a* obtained with the method proposed in the paper (average values column) and the experimental value obtained from the instantaneous retardance values (inst. values column), and for the two working geometries.

	With NPBS			Quasiperpendicular		
	Average values		Inst. values	Average values		Inst. values
Sequence	Γ_{diff} (deg)	Fluct. amplit. (deg)	Fluct. amplit. (deg)	Γ_{diff} (deg)	Fluct. amplit. (deg)	Fluct. amplit. (deg)
18_6 default	11	20 (GL 16)	20 (GL 16)	15	27 (GL 17)	28 (GL17)
	47	84 (GL 61)	92 (GL 61)	42	75 (GL 66)	88 (GL 66)
	52	92 (GL 170)	—	51	91 (GL 175)	—
18_6 linear	6	11 (GL 16)	18 (GL 16)	10	18 (GL 22)	17 (GL 22)
	30	52 (GL 131)	59 (GL 131)	27	47 (GL 130)	51 (GL 130)
5_5 linear	6	11 (GL 26)	17 (GL26)	11	19 (GL 32)	17 (GL32)
	21	38 (GL 153)	44 (GL 153)	19	34 (GL 146)	37 (GL 146)

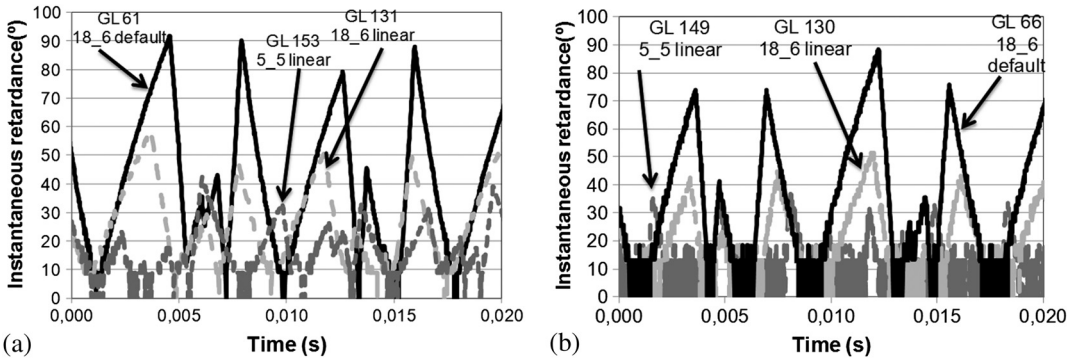

Fig. 8 Temporal evolution of the retardance at gray levels, indicated on the figure, corresponding to the second extremals in the plots in Figs. 7(b) and 7(d) and for the three sequences. (a) and (b) correspond, respectively, to the setup with the NPBS and to quasiperpendicular incidence.

method we propose and the one obtained from the instantaneous retardance values that we measure. This is true for the two working geometries.

Once the fluctuation amplitude values have been validated, we can introduce them in Eq. (11) to calculate the average retardance. What we do is to extrapolate the fluctuation amplitude value calculated from the extremals to a wider gray-level range: the fluctuation amplitude value from the first extremal is considered to be roughly valid until half of the gray-level distance between the two extremals, and from there, the value from the second extremal is the one considered valid, and so on.

In Figs. 9(a) to 9(c), we show, respectively, for the three sequences the average retardance value calculated with this procedure as a function of the gray level. They correspond to the "corrected" curve (continuous line) in the legend. The "uncorrected" (dashed line) correspond to the calculated retardance already plotted in Figs. 7(b) and 7(d). In the graphs we plot the results for the two working geometries considered, NPBS and quasiperpendicular. In the case of the sequence 18-6 default [Fig. 9(a)], deviations are very large between corrected and uncorrected curves for most of the gray-level range. However, in the case of the sequences 18-6 2pi linear 633 nm and 5-5 2pi linear 633 nm [Figs. 8(b) and 8(c)], deviations are only encountered in the proximity of the extremals, which means that applicability of the classical expression given in Eq. (5) may still be possible in many situations in spite of the existence of phase flicker. We also appreciate that results obtained for both working geometries practically overlap. This indicates that polarization effects produced by the NPBS in front of the LCoS and obliquity effects in the case of quasiperpendicular incidence are very small. Therefore, the extended linear polarimeter technique we have proposed in the paper is a robust method to obtain the average linear retardance for devices exhibiting fluctuations or instabilities in their linear retardance.

4 Conclusions

We have shown the applicability of the classical and well-established linear polarimeter to the measurement of linear retardance in the presence of phase flicker. This analysis shows that there may exist large errors in the results provided by the linear polarimeter when measuring the linear retardance of a device. However, these errors depend on the specific retardance value under measurement, being a maximum when at retardance points multiple of 180 deg. We show that these specific points, instead of being a limitation, offer the opportunity to measure the fluctuation amplitude consistently. An elegant method is further proposed enabling the measurement of the average retardance value, thus extending the applicability of the classical linear polarimeter to a new range of samples. The method is both simple and does not require especial or expensive equipment. Validation of the technique has been accomplished with a setup enabling both average and instantaneous retardance measurements. We have analyzed the applicability of the technique for two different working geometries enabling to separate incident and reflected beams. Results obtained indicate that polarization effects produced by the NPBS in front of the

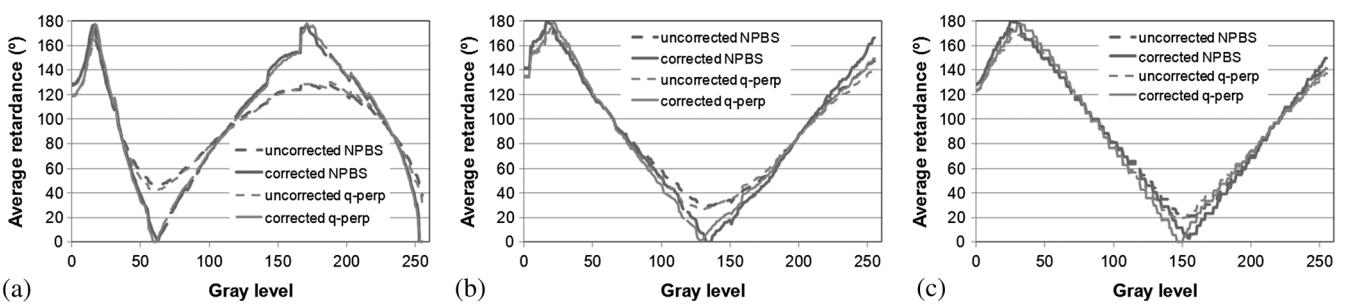

Fig. 9 Average retardance versus gray level when considering the classical (uncorrected curves) and the extended (corrected curves) linear polarimeter technique proposed in the paper, for both the NPBS and the quasiperpendicular geometries. (a) 18-6 default; (b) 18-6 2pi linear 633 nm; (c) 5-5 2pi linear 633 nm.

LCoS and obliquity effects in the case of quasiperpendicular incidence are very small. Therefore, the extended linear polarimeter technique we have proposed in the paper is a robust method to obtain the average linear retardance for devices exhibiting fluctuations or instabilities in their linear retardance. As a final remark, specifically for the LCoS analysis performed, we note that the sequences considered in this work enable to attain a dynamic retardance range of 360 deg or even larger. In the case of the sequence 5-5 2pi linear 633 nm, the amplitude of the fluctuations is basically <30 deg. In the case of blazed gratings, this enables diffraction efficiencies >95% [see the work of Lizana et al.,[18] Fig. 3(b)]. Therefore, existence of fluctuations is not in itself a problem. Proper characterization enables to find the optimal sequence as shown in the paper.

Acknowledgments

This work was supported by the Ministerio de Trabajo y Competitividad of Spain (projects FIS2011-29803-C02-01 and FIS2011-29803-C02-02), by the Generalitat Valenciana of Spain (projects PROMETEO/2011/021 and ISIC/2012/013), and by Universidad de Alicante (project GRE12-14).

References

1. J. Turunen and F. Wyrowski, Eds., *Diffractive Optics for Industrial and Commercial Applications*, Akademie Verlag, Berlin (1997).
2. H. J. Coufal, D. Psaltis, and B. T. Sincerbox, Eds., *Holographic Data Storage*, Springer-Verlag, Berlin (2000).
3. W. Osten, C. Kohler, and J. Liesener, "Evaluation and application of spatial light modulators for optical metrology," *Opt. Pura Apl.* **38**, 71–81 (2005).
4. S. T. Wu and D. K. Yang, *Reflective Liquid Crystal Displays*, John Wiley & Sons Inc., Chichester (2005).
5. N. Collings et al., "The applications and technology of phase-only liquid crystal on silicon devices," *J. Display Technol.* **7**, 112–119 (2011).
6. J. E. Wolfe and R. A. Chipman, "Polarimetric characterization of liquid-crystal-on-silicon panels," *Appl. Opt.* **45**, 1688–1703 (2006).
7. A. Márquez et al., "Mueller-Stokes characterization and optimization of a liquid crystal on silicon display showing depolarization," *Opt. Express* **16**, 1669–1685 (2008).
8. P. Clemente et al., "Use of polar decomposition of Mueller matrices for optimizing the phase response of a liquid-crystal-on-silicon display," *Opt. Express* **16**, 1965–1974 (2008).
9. A. Lizana et al., "Wavelength dependence of polarimetric and phase-shift characterization of a liquid crystal on silicon display," *J. Eur. Opt. Soc.* **3**, 08012 (2008).
10. A. Lizana et al., "Time-resolved Mueller matrix analysis of a liquid crystal on silicon display," *Appl. Opt.* **47**, 4267–4274 (2008).
11. J. García-Márquez et al., "Flicker minimization in an LCoS spatial light modulator," *Opt. Express* **20**, 8431–8441 (2012).
12. A. Lizana et al., "Influence of the temporal fluctuations phenomena on the ECB LCoS performance," *Proc. SPIE* **7442**, 74420G (2009).
13. A. Hermerschmidt et al., "Wave front generation using a phase-only modulating liquid-crystal based micro-display with HDTV resolution," *Proc. SPIE* **6584**, 65840E (2007).
14. J. R. Moore et al., "The silicon backplane design for an LCOS polarization-insensitive phase hologram SLM," *IEEE Photon. Techol. Lett.* **20**, 60–62 (2008).
15. A. Márquez et al., "Classical polarimetric method revisited to analyse the modulation capabilities of parallel aligned liquid crystal on silicon displays," *Proc. SPIE* **8498**, 84980L (2012).
16. C. Ramirez et al., "Point diffraction interferometer with a liquid crystal monopixel," *Opt. Express* **21**, 8116–8124 (2013).
17. A. Lizana et al., "Time fluctuations of the phase modulation in a liquid crystal on silicon display: characterization and effects in diffractive optics," *Opt. Express* **16**, 16711–16722 (2008).
18. A. Lizana et al., "The minimum Euclidean distance principle applied to improve the modulation diffraction efficiency in digitally controlled spatial light modulators," *Opt. Express* **18**, 10581–10593 (2010).
19. L. Yao, Z. Zhiyao, and W. Runwen, "Optical heterodyne measurement of the phase retardation of a quarter-wave plate," *Opt. Lett.* **13**, 553–555 (1988).
20. L.-H. Shyu, C.-L. Chen, and D.-C. Su, "Method for measuring the retardation of a wave plate," *Appl. Opt.* **32**, 4228–4230 (1993).
21. A. Márquez et al., "Phase measurements of a twisted nematic liquid crystal spatial light modulator with a common-path interferometer," *Opt. Commun.* **190**, 129–133 (2001).
22. S. Nakadate, "High precision retardation measurement using phase detection of Young's fringes," *Appl. Opt.* **29**, 242–246 (1990).
23. H. G. Jerrard, "Transmission of light through birefringent and optically active media: the Poincaré sphere," *J. Opt. Soc. Am.* **44**, 634–640 (1954).
24. P. Kurzynowski, "Senarmont compensator for elliptically birefringent media," *Opt. Commun.* **197**, 235–238 (2001).
25. G. Goldstein, *Polarized Light*, Marcel Dekker, New York (2003).
26. N. G. Theofanous, "Error analysis of circular polarizer-analyzer systems for phase retardation measurements," *J. Opt. Soc. Am. A* **4**, 2191–2200 (1987).
27. P. A. Williams, A. H. Rose, and C. M. Wang, "Rotating-polarizer polarimeter for accurate retardance measurement," *Appl. Opt.* **36**, 6466–6472 (1997).
28. M. Born and E. Wolf, *Principles of Optics*, 7th ed., pp. 823–826, Cambridge University, Cambridge (1999).
29. A. Márquez et al., "Characterization of the retardance of a wave plate to increase the robustness of amplitude-only and phase-only modulations of a liquid crystal display," *J. Mod. Opt.* **52**, 633–650 (2005).
30. C. Ramirez et al., "Polarimetric method for liquid crystal displays characterization in presence of phase fluctuations," *Opt. Express* **21**, 3182–3192 (2013).
31. A. Lizana et al., "Influence of the incident angle in the performance of liquid crystal on silicon displays," *Opt. Express* **17**, 8491–8505 (2009).

Francisco J. Martínez received his BS degree in electronic engineering from University of Valencia in 1996 and his BS degree in physics in 1999. Currently, he is a research assistant with the Applied Physics to Science and Technology Institute from University of Alicante, and assistant professor of electronics in Miguel Hernandez University. His research interests include diffractive optics and holography.

Andrés Márquez received his MSc and PhD degrees in physics from Universidad Autónoma de Barcelona in 1997 and 2001, respectively. In 2000, he joined the Universidad de Alicante, where he is an associate professor of applied physics. His research interests include holographic recording materials, liquid crystal spatial light modulators, optical image processing, and diffractive optics.

Sergi Gallego obtained his degree in physics at University of Valencia in 2001 and his PhD at the University of Alicante, Spain, in 2005, where he works as lecturer. His research interests include holographic recording materials, diffraction, liquid crystal displays applied to holography, diffractive elements, and photopolymers. He has authored or coauthored one patent and more than 60 publications in renowned international journals (journals in the JCR of ISI).

Jorge Francés received his PhD degree at the University of Alicante in 2011. He received his MSEE in 2009 and his BSEE in 2006, both from the Technical University of Valencia, Valencia, Spain. He has been working as an assistant lecturer with the University of Alicante since 2008. His main research interests include physical optics, sound and vibration, and numerical simulation.

Inmaculada Pascual received her MSc degree in physics from the University of Granada in 1985 and her PhD degree from the University of Valencia in 1990. She is a full professor of optics at the University of Alicante. She has carried out research in holography, mainly on holographic recording material, holographic optical elements, and optical data storage. She has published more than 125 papers and presented more than 170 papers in scientific conferences.